Facile One-Pot Synthesis of Mesoporous SnO_2 Microspheres via Nanoparticles Assembly and Lithium Storage Properties

Rezan Demir-Cakan,[†] Yong-Sheng Hu,*[,‡] Markus Antonietti,[†] Joachim Maier,*[,‡] and Maria-Magdalena Titirici*[,†]

Max Planck Institute for Colloids and Interfaces, Am Muehlenberg 1, 14476 Golm, Germany, and Max Planck Institute for Solid State Research, Heisenbergstrasse 1, 70569 Stuttgard, Germany

Received November 1, 2007
Revised Manuscript Received January 11, 2008

Materials based on the wide-bandgap n-type semiconductor SnO_2 have raised great interest for various technologically important applications in gas sensing,[1a,b,2] catalysis[3] as well as in lithium batteries.[4–8] In the past few years, a wide variety of SnO_2 nanostructures, such as nanoparticles,[9] nanorods/nanowires,[10] nanotubes,[11] hollow spheres,[12] or mesoporous structures[13] have been prepared using sol–gel,[14] thermal-evaporation,[15] laser-ablation,[16] or nonaqueous synthesis.[13a] Porosity on the nanometric scale is an important attribute for electrochemical storage devices such as lithium batteries. Porous materials with large pore diameter have good electrolyte accessibility; therefore, ionic transport is facilitated, which in many cases leads to a substantial improvement of the rate capability (i.e., power density).

Carbonaceous materials can be produced using hydrothermal carbonization (HTC), which is now already a well-established method to create hydrophilic carbon materials starting from water soluble carbohydrates.[17–19] A simplified reaction mechanism of the formation of the carbon spheres involves the dehydration of the carbohydrate in the first step and subsequent polymerization and carbonization of the so-formed organic compounds in the second step. The resulting droplets form either the final spherical carbon particles or they can be used for nanocoating other structures.[20,21] Here, we report the facile one-pot synthesis of mesoporous SnO_2 microspheres using hydrothermal carbonization of furfural in the presence of SnO_2 nanoparticle sols. The preparation of the SnO_2 sol is described elsewhere.[13a]

During the hydrothermal carbonization in the presence of SnO_2 nanoparticles, those nanoparticles are uniformly distributed into the resulting hydrophilic carbon spheres (Figure 1). After the removal of the carbon matrix, the SnO_2 nanoparticles assemble together into mesoporous SnO_2 microspheres (Figure 2). This procedure represents a facile route to uniformly incorporate nanoparticles into carbon microspheres.The size of these microspheres can be tunned depending on the concentration of furfural, the time and the temperature of the hydrothermal reaction.[18] These carbon/nanoparticle composites exhibit themselves interesting electrochemical properties. However, this study is the subject of a future publication. Here, we want to focus on the synthesis of mesoporous SnO_2 microspheres by easy assembly of individual SnO_2 nanoparticles using hydrothermal carbon microspheres as sacrificial templates. The advantage of having micrometer-sized mesoporous SnO_2 particles,

* Corresponding author. E-mail: Magdalena.Titirici@mpikg.mpg.de (M.-M.T.); Y.Hu@fkf.mpg.de (Y.-S.H.).
[†] Max Planck Institute for Colloids and Interfaces.
[‡] Max Planck Institute for Solid State Research.

(1) (a) Tzou, H. S.; Lee, H. J.; Arnold, S. M. *Mech. Adv. Mater. Struc.* **2004**, *11*, 367. (b) Scott, R. W. J.; Yang, S. M.; Chabanis, G.; Coombs, N.; Williams, D. E.; Ozin, G. A. *Adv. Mater.* **2001**, *13*, 1468.
(2) Jamnik, J.; Kamp, B.; Merkle, R. *Solid State Ionics* **2002**, *150*, 157.
(3) Her, Y. S.; Matijevic, E.; Chon, M. C. *J. Mater. Res.* **1995**, *10*, 3106.
(4) Idota, Y.; Kubota, T.; Matsufuji, A.; Maekawa, Y.; Miyasaka, T. *Science* **1997**, *276*, 1395.
(5) (a) Winter, M.; Besenhard, O. J.; Spahr, M. E.; Novak, P. *Adv. Mater.* **1998**, *10*, 725. (b) Yang, J.; Winter, M.; Besenhard, J. O. *Solid State Ionics* **1996**, *90*, 281. (c) Besebhard, J. O.; Yang, J.; Winter, M. *J. Power Sources* **1997**, *68*, 87. (d) Courtney, I. A.; Dahn, J. R. *J. Electrochem. Soc.* **1997**, *144*, 2943. (e) Mao, O.; Dunlap, R. A.; Dahn, J. R. *J. Electrochem. Soc.* **1999**, *146*, 405.
(6) (a) Li, H.; Huang, X. J.; Chen, L. Q. *Electrochem. Solid-State Lett.* **1998**, *1*, 241. (b) Shi, L. H.; Li, H.; Wang, Z. X.; Huang, X. J.; Chen, L. Q. *J. Mater. Chem.* **2001**, *11*, 1502. (c) Li, H.; Shi, L. H.; Wang, Q.; Chen, L. Q.; Huang, X. J. *Solid State Ionics* **2002**, *148*, 247.
(7) (a) Lee, K. T.; Jung, Y. S.; Oh, S. M. *J. Am. Chem. Soc.* **2003**, *125*, 5625. (b) Jung, Y. S.; Lee, K. T.; Ryu, J. H.; Im, D.; Oh, S. M. *J. Electrochem. Soc.* **2005**, *152*, A1452. (c) Han, S.; Jang, B.; Kim, T.; Oh, S. M.; Hyeon, T. *Adv. Funct. Mater.* **2005**, *15*, 1845.
(8) (a) Yan, H.; Sokolv, S.; Lytle, J. C.; Stein, A.; Zhang, F.; Smyrl, W. H. *J. Electrochem. Soc.* **2003**, *150*, A1102. (b) Lee, K. T.; Lytle, J. C.; Ergang, N. S.; Oh, S. M.; Stein, A. *Adv. Funct. Mater.* **2005**, *15*, 547. (c) Li, N. C.; Martin, C. R. *J. Electrochem. Soc.* **2001**, *148*, A164. (d) Pereira, N.; Klein, L. C.; Amatucci, G. G. *Solid State Ionics* **2004**, *167*, 29.
(9) (a) Juttukonda, V.; Paddock, R. L.; Raymond, J. E.; Denomme, D.; Richardson, A. E.; Slusher, L. E.; Fahlman, B. D. *J. Am. Chem. Soc.* **2006**, *128*, 420. (b) Ahn, H. J.; Choi, H. C.; Park, K. W.; Kim, S. B.; Sung, Y. E. *J. Phys. Chem B* **2004**, *108*, 9815.
(10) (a) Chen, D.; Gao, L. *Chem. Phys. Lett.* **2004**, *398*, 201. (b) Cheng, B.; Rusell, J. M.; Shi, W.; Zhang, L.; Samulski, E. T. *J. Am. Chem. Soc.* **2004**, *126*, 5972. (c) Park, M. S.; Wang, G. X.; Kang, Y. M.; Wexler, D.; Dou, S. X.; Liu, H. K. *Angew. Chem., Int. Ed.* **2007**, *46*, 750.
(11) (a) Zhao, L.; Yosef, M.; Steinhart, M.; Goring, P.; Hofmeister, H.; Gosele, U.; Schlecht, S. *Angew. Chem., Int. Ed.* **2005**, *44*, 311. (b) Wang, Y.; Zeng, H. C.; Lee, J. Y. *Adv. Mater.* **2006**, *18*, 645.
(12) (a) Zhong, Z.; Yin, Y.; Gates, B.; Xia, Y. *Adv. Mater.* **2000**, *12*, 206. (b) Shao, W. P.; Wang, Z. H.; Zhang, Y. G.; Cui, J. H.; Yu, W. C.; Qian, Y. T. *Chem. Lett.* **2005**, *44*, 4342. (c) Lou, X. W.; Wang, Y.; Yuan, C.; Lee, J. Y.; Archer, L. A. *Adv. Mater.* **2006**, *18*, 2325.
(13) (a) Ba, J.; Polleux, J.; Antonietti, M.; Niederberger, M. *Adv. Mater.* **2005**, *17*, 2509. (b) Fan, J.; Wang, T.; Yu, C.; Tu, B.; Jiang, Z.; Zhao, D. *Adv. Mater.* **2004**, *16*, 1432. (c) Yu, S.; Frech, R. *J. Power Sources* **2002**, *104*, 97. (d) He, Z. Q.; Li, X. H.; Xiong, L. Z.; Wu, X. M.; Xiao, Z. B.; Ma, M. Y. *Mater. Res. Bull.* **2005**, *40*, 861. (e) Park, M. S.; Wang, G. X.; Kang, Y. M.; Kim, S. Y.; Liu, H. K.; Dou, S. X. *Electrochem. Commun.* **2007**, *9*, 71.
(14) (a) de Monredon, S.; Cellot, A.; Ribot, F.; Sanchez, C.; Armelao, L.; Gueneau, L.; Delattre, L. *J. Mater. Chem.* **2002**, *12*, 2396. (b) Pinna, N.; Neri, G.; Antonietti, M.; Niederberger, M. *Angew. Chem., Int. Ed* **.2004**, *43*, 4345.
(15) Dai, Z. R.; Pan, Z. W.; Wang, Z. L. *Adv. Funct. Mater.* **2003**, *13*, 9.
(16) Hu, J.; Bando, Y.; Liu, Q.; Golberg, D. *Adv. Funct. Mater.* **2003**, *13*, 493.
(17) Wang, Q.; Li, H.; Chen, L.; Huang, X. *Carbon* **2001**, *39*, 2211.
(18) Sun, X. M.; Li, Y. D. *Angew. Chem., Int. Ed.* **2004**, *43*, 597.
(19) Titirici, M. M.; Antonietti, M.; Thomas, A. *Chem. Mater.* **2006**, *18*, 3808.
(20) Qian, H. S.; Yu, S. H.; Luo, L.; Gong, J.; Liu, X.; Fei, L. *Chem. Mater.* **2006**, *18*, 2102.
(21) Titirici, M. M.; Thomas, A.; Antonietti, M. *Adv. Funct. Mater.* **2007**, *17*, 1010.

10.1021/cm7031288 CCC: $40.75
Published on Web 01/30/2008

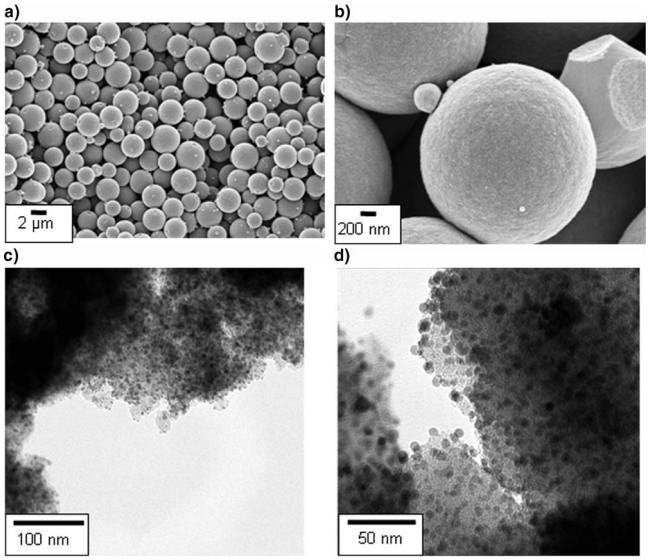

Figure 1. (a, b) SEM micrographs of the hydrothermal carbon/ SnO_2 composites spheres; (c, d) TEM micrographs of microtomed carbon/ SnO_2 composites structures showing cross-sections of the as-formed structures.

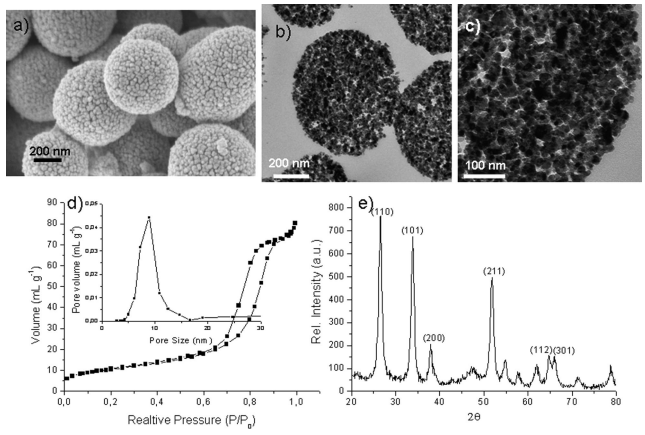

Figure 2. (a) SEM micograph of the SnO_2 composed of agglomerated nanoparticle; (b, c) TEM microtommed micrographs of the SnO_2 microspheres showing the porous structure resulting upon agglomeration of the nanoparticles; (d) adsorption–desorption isotherm and pore size distribution of the SnO_2 microspheres, (e) XRD pattern of the mesoporous SnO_2 microspheres.

besides the resulting mesoporosity, lies in a more easy handling of the particles, for example, to produce an electrode–film. This is due to the fact that micrometer-sized spheres possess a higher packing density then the individual nanoparticles, which easily tend to agglomerate. Figure 1 shows the SEM/TEM micrographs of the SnO_2/carbon composites obtained after the hydrothermal carbonization of furfural in the presence of the SnO_2 nanoparticles. Carbon spheres of around 3 μm enclosing SnO_2 nanoparticles were obtained. According to the TGA, the SnO_2 nanoparticles inside the carbon matrix amounts 60%. (see the Supporting Information, Figure S1a). The distribution of the SnO_2 inside the carbon matrix could be visualized using TEM microtoming. Thus the cross-section of the carbon spheres reveals that the SnO_2 nanoparticles are well distributed inside the carbon matrix meaning that they got perfectly dispersed in the monomer phase.

After the carbon matrix is removed, the SEM and TEM micrographs show that the spheres are formed out of aggregated SnO_2 nanoparticles (images a and b in Figure 2). The size of the resulting mesoporous SnO_2 microspheres shrinks in comparison with the carbon composites upon removal of the carbon matrix. As the microspheres are composed of SnO_2 nanoparticles, a high surface area can be expected. This was proven by nitrogen adsorption experiments. The adsorption–desorption isotherm is given in Figure 2d showing a hysteresis loop characteristic to mesoporous materials. According to the BET method, the resulting SnO_2 microspheres have a specific surface area of 70 m^2/g. The apparently low specific surface area is due to the high density of SnO_2 (6.95 g/cm^3). The material shows a pore size distribution around 10 nm calculated from the adsorption brunch of the isotherm using the BJH model. The porosity corresponds to the interstitial pores formed between nanoparticles upon agglomeration. As the size of the individual SnO_2 nanoparticles lies between 3 and 7 nm and are rather monodisperse (see the Supporting Information, Figure S2), we can deduce that the nanoparticles first aggregate in the calcination step to extended aggregates, which form after the final mesoporous structure.This is supported also by the cross-section microtommed TEM pictures in images b and c in Figure 2, where we can see that the nanoparticle aggregates forming the interstitial pores are about 15 nm in size in comparison with the 3–7 nm initial size size (see the Supporting Information, Figure S2). The porous structure resulting upon aggregation of the nanoparticles can also be clearly seen from the microtommed TEM micrographs (images b and c in Figure 2).

According to the TGA analysis, all the carbon has been successfully removed during the calcination process. (see the Supporting Information, Figure S1b). However, this process is likely to contribute to some extend to the overall porosity of the resulting material.

The XRD pattern of the final SnO_2 mesoporous microspheres is displayed in Figure 2e and corresponds, as in the case of individual nanoparticles, to the cassiterite structure. This means that the calcination and removal of the sacrificial carbon template essentially leaves the crystallinity unaffected.

To test the potential applicability of the as-synthesized mesoporous SnO_2 microspheres in lithium batteries, we investigated the storage properties with respect to Li insertion/extraction. Galvanostatic discharge–charge and cyclic voltammogram (CV) experiments were carried out in different voltage ranges. For comparison, in addition to the mesoscopic SnO_2 microsphere, commercially available nonporous micrometer-sized SnO_2 was also tested under the same electrochemical condition. The physical characterization of this sample (SEM, XRD, BET) is given in Figure S3 of the Supporting Information.

The discharge (Li insertion)/charge (Li extraction) curves (Figure 3a) of the mesoporous SnO_2 electrode were obtained in 1 M $LiPF_6$ EC/DMC electrolyte solution at a current density of 100 mA g^{-1}. As regards the first cycle, the mesoporous SnO_2 microspheres show much higher reversible capacity ($\sim$960 mA h g^{-1}) in the voltage range of 0.02 to 2.5 V when compared with the nonporous SnO_2 sample

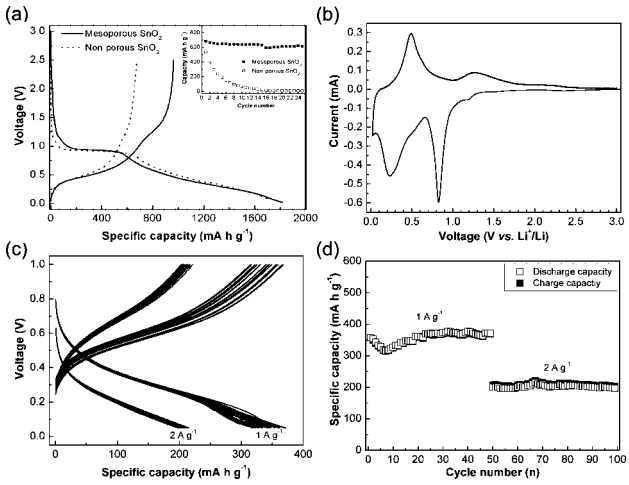

Figure 3. (a) First discharge/charge profiles for the mesoporous SnO_2 and microsized SnO_2 samples cycled at a current density of 100 mA g^{-1}, inset shows the cycling performance of both samples cycled between voltage limits of 0.05 and 1V; (b) cyclic voltammogram of the mesoporous SnO_2 at a scan rate of 0.05 mV/s; (c) discharge/charge profiles for the mesoporous SnO_2 sample cycled between voltage limits of 0.05 and 1V at current densities of 1 and 2 A g^{-1}; (d) variation in discharge/charge capacity versus cycle number for the mesoporous SnO_2 sample cycled at current densities of 1 and 2 A g^{-1}.

($\sim$ 670 mA h g^{-1}). Furthermore, the mesoporous SnO_2 microspheres exhibit an initial Coulombic efficiency of about 53%, which is remarkably higher than the nonporous SnO_2 (39%) and other reports.[10c,13b–e] When the voltage was limited between 0.05 and 1 V, the mesoporous SnO_2 microspheres exhibit much better cycling performance with a reversible capacity of around 600 mA h g^{-1} than that of nonporous SnO_2 sample, as shown in the inset of Figure 3a. Figure 3b presents the CV curve of the mesoporous SnO_2 microspheres. Three obvious reduction peaks are present around 1.2, 0.83, and 0.24 V. These peaks can be ascribed to the formation of the solid electrolyte interphase (SEI, eq 1), the decomposition of SnO_2 to Sn and Li_2O nanocomposite (eq 2), and finally the alloying reaction between Sn and Li (eq 3),[5,6,22,23] respectively

$$Li^+ + e^- + \text{electrolyte} \rightarrow \text{SEI(Li)} \quad (1)$$

$$SnO_2 + 4Li^+ + 4e^- \rightarrow Sn + 2Li_2O \quad (2)$$

$$Sn + xLi^+ + xe^- \leftrightarrow Li_xSn \quad (0 \le x \le 4.4) \quad (3)$$

It is generally accepted that the first two reactions are not reversible and should be responsible for the large irreversible capacity of the first cycle.[5] However, the alloying reaction between Sn and Li is highly reversible, as corroborated by the observation of an oxidation peak at 0.48 V in Figure 3b. Note that an oxidation peak around 1.27 V was also observed for the mesoporous SnO_2 microspheres, which is most likely due to the part reversible reaction of eq 2 because the Li−Sn alloying-dealloying reactions only occur below 1.0 V. [4,5]This point needs to be further studied by other techniques.

Furthermore, the mesoporous SnO_2 microspheres allow for discharging/charging at higher current densities. It can be seen from panels c and d in Figure 3 that the stable reversible capacities are around 370 and 200 mA h g^{-1} at the current densities of 1 and 2 A g^{-1}, respectively. The significant improvement of the electrochemical performance is attributed to the unique mesoporous structure of SnO_2 microspheres with a variety of favorable properties: the 10 nm mesopores promise to render the liquid electrolyte diffusion into the bulk of the electrode material facile and hence to provide fast transport channels for the conductive ions (e.g., solvated Li^+ ions); they are expected to buffer well against the local volume change during the Li−Sn alloying−dealloying reactions, whereas the nanosized building blocks (about 3–7 nm) should provide a low absolute volume change during the Li−Sn alloying−dealloying reactions; the short diffusion length for Li insertion are beneficial in retaining the structural stability as well as leading to a good cycling performance and high rate capability.

In conclusion, we have developed a simple and surfactant-free method to prepare mesoporous SnO_2 microspheres by using hydrothermal carbonization of furfural in the presence of SnO_2 nanoparticles. The resulting hydrophilic carbon microspheres contain well-dispersed SnO_2 nanoparticles in their composition. Upon removal of the carbon matrix, these nanoparticles assemble together into mesoporous microspheres. The micrometer-sized spheres enable easy handling in terms of separation or film formation in comparison with their nanosized constituents, whereas their resulting mesoporosity provides a network that could be easily penetrated by the electrolyte. This porosity in combination with the nanosized building blocks results in significant improvement of the electrochemical performance when compared with a nonporous micrometer-sized commercially available SnO_2 sample.

Acknowledgment. The authors are indebted to MPG-ENERCHEM project.

Supporting Information Available: Figures S1−S3 and experimental details (PDF). This material is available free of charge via the Internet at http://pubs.acs.org.

CM7031288

(22) Hosono, E.; Matsuda, H.; Honma, I.; Ichihara, M.; Zhou, H. S. *J. Electrochem. Soc.* **2007**, *154*, A146.
(23) (a) Hassoun, J.; Panero, S.; Simon, P.; Taberna, P. L.; Scrosati, B. *Adv. Mater.* **2007**, *19*, 1632. (b) Derrien, G.; Hassoun, J.; Panero, S.; Scrosati, B. *Adv. Mater.* **2007**, *19*, 2336.